Theoretical insight on PTB7:PC 71 BM, PTB7-th:PC 71 BM and Si-PCPDTBT:PC 71 BM interactions governing blend nanoscale morphology for efficient solar cells

Claudia Caddeo, Alessio Filippetti, Andrea Bosin, Christine Videlot-Ackermann, Jörg Ackermann, Alessandro Mattoni

Theoretical insight on PTB7:$PC_{71}BM$, PTB7-th:$PC_{71}BM$ and Si-PCPDTBT:$PC_{71}BM$ interactions governing blend nanoscale morphology for efficient solar cells

Claudia Caddeo[a], Alessio Filippetti[a,b], Andrea Bosin[b], Christine Videlot-Ackermann[c], Jörg Ackermann[†c], Alessandro Mattoni[*a]

[a]*Istituto Officina dei Materiali (CNR - IOM) Cagliari, Cittadella Universitaria, I-09042 Monserrato (Ca), Italy*
[*]*mattoni@iom.cnr.it*
[b]*Dipartimento di Fisica, Università degli Studi di Cagliari, Cittadella Universitaria, I-09042 Monserrato (Ca), Italy*
[c]*Aix Marseille Univ., UMR CNRS 7325, CINaM, 13288 Marseille, France*
[†]*jorg.ackermann@univ-amu.fr*

Abstract

The nanoscale morphology of solution processed bulk heterojunctions is governed by miscibility of donor and acceptor in the selected solvent and drying of the layer during processing. Ternary blends are of great interest for high efficiency polymer solar cells, but prediction of their morphology is highly complex. Here we perform atomistic simulations to study the miscibility of three different polymers of interest for ternary organic photovoltaics (the small band gap polymers PTB7 and PTB7-th, and the sensitizer Si-PCPDTBT) with the fullerene acceptor $PC_{71}BM$.The free energy of mixing of fullerenes with polymers is calculated as a function of the relative concentration. The blend density is also varied to simulate out-of-equilibrium conditions occurring during layer processing. By analyzing the results within the Flory-Huggins theory we find that, for a specific range of fullerene weight ratios and densely packed blends the sensitizer is most likely located in the host polymer phase due to its low miscibility with the fullerene. This configuration is the preferred one for the solar cell in order to deactivate hole traps typically formed in the binary blends and reduce recombination. Notably, we find that these results can be different qualitatively at lower density and out-of-equilibrium blends. This work shows that weight ratios and density can be in principle chosen to select specific morphologies in ternary organic blends.

Keywords: thermodynamics of polymers, atomistic simulations, organic photovoltaics, fullerene, ternary solar cells, low band gap polymers

1. Introduction

Since the first observations of photoconductivity in organic materials[1], the scientific interest in organic solar cells (OSCs) as important candidates for a reliable and economically viable renewable energy technology has increased enormously[2, 3, 4, 5]. Polymer-based solar cells (PSC), typically composed of a polymer donor and an organic acceptor, are widely studied for their light weight, flexibility and easy solution-based processing. However, these cells still present some issues which prevent their wide distribution in the market[6, 7]. Their power conversion efficiency (PCE) is still relatively low, mainly due to carrier recombination[8, 9], and they have low thermal stability and can decompose when heated, for example due the segregation of acceptor $PC_{61}BM$[1] at moderately

[1] [6,6]-phenyl-C61- butyric acid methyl ester

high temperatures [10, 11, 12, 13].

Among fullerene based organic solar cells, high efficiency devices have been obtained with either PTB7[2] or PTB7-th[3] polymers (Fig. 1, left). These polymers are typically mixed with the fullerene derivative $PC_{71}BM$[4] which is preferred to $PC_{61}BM$ due to the better miscibility and reduced tendency to segregate[14].

The PCE of a solar cell is related to the short-circuit current density (J_{sc}), the open-circuit voltage (V_{oc}) and the fill factor (*FF*). The J_{sc} is strongly dependent on the sunlight harvesting efficiency, thus a strategy to improve the values of the short-circuit current is to introduce additional light absorbing components in the blend, in order to cover a wider portion of the solar spectrum.

Organic blends, formed by two donors (with complementary absorption profile[15, 16]) and one acceptor (or one donor and two acceptors) have shown to enhance sizably the J_{sc} [17, 18]. Furthermore, by a suitable choice of the components, the position of the highest occupied/lowest unoccupied molecular orbital (HOMO/LUMO) levels can be tuned to improve V_{oc}[19, 20]. Currently, the record PCEs for such organic ternary blends is around 16% [21]. One of the limiting factors for efficiency is the *FF*, that is is typically reduced due to the increased carrier recombination in presence of a third component[22, 23, 24, 25, 18].

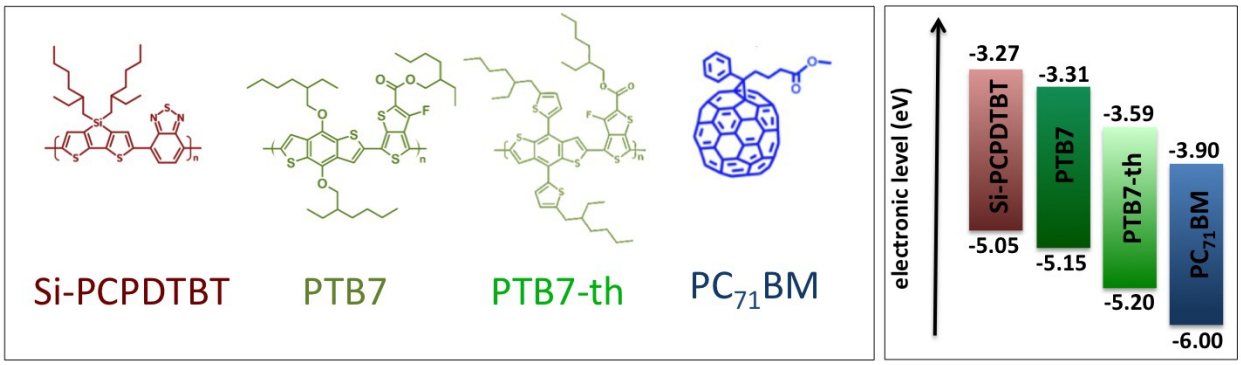

Figure 1: Left panel: chemical structure of the studied materials; right panel: electronic level alignment. The values of the energy levels are taken from literature[26, 27]

Recently, efficient blends have been realized by introducing a small amount of polymer Si-PCPDTBT[5] as sensitizer in PTB7:$PC_{71}BM$ and PTB7-th:$PC_{71}BM$ cells (Fig. 1, left); these cells have shown a remarkably high *FF* of 77% and 71%, respectively[26]. Similar improvements have been obtained also in the case of non-fullerene acceptors[20]. The high values of *FF* are attributed to the reduction of trap-assisted recombination, associated to an enhanced charge transport. The proposed mechanism involves hole transfer from the host (PTB7 or PTB7-th) to the sensitizer Si-PCPDTBT which keeps the holes separated from the fullerenes until they are collected at electrodes[26]. Given the relative energy level alignment of the three components (Fig. 1, right), it is required that the Si-PCPDTBT sensitizer is spatially separated from fullerene phase. The realization of such a morphology with optimized fill factor requires to understand and to control the relative miscibilities and in particular that of sensitizer and host polymer with the fullerenes.

[2]Poly[[4,8-bis[(2-ethylhexyl)oxy]benzo[1,2-b:4,5-b']dithiophene-2,6-diyl][3-fluoro-2-[(2-ethylhexyl)carbonyl]thieno[3,4-b]thiophenediyl]]

[3]Poly[4,8-bis(5-(2-ethylhexyl)thiophen-2-yl)benzo[1,2-b;4,5-b']dithiophene-2,6-diyl-alt-(4-(2-ethylhexyl)-3-fluorothieno[3,4-b]thiophene-)-2-carboxylate-2-6-diyl)]

[4][6,6]-phenyl-C71- butyric acid methyl ester

[5]Poly[4,4-bis(2-ethylhexyl)-dithieno[3,2-b:2',3'-d]silole)-2,6-diyl-al-(2,1,3-benzothiadiazole)-4,7-diyl]

The importance of miscibility to control morphology and performances was already pointed out for binary solar cells based on Si-PCPDTBT[28, 29, 30, 31, 8, 32, 33].

In the light of these findings, as a first-step towards the modeling of complex ternary blends, it is of primary importance to study comparatively the binary interactions and miscibility of different polymers with fullerenes and to clarify the physical quantities (such as the concentration and density) that control the miscibility and the interfaces. Atomistic simulations, thanks to the available computing power, are nowadays able to study polymer solutions[34, 35, 36, 37, 33, 38, 39]. For example, Wang et al.[33] have investigated the polymer self-aggregation, polymer-fullerene packing and fullerene connecting networks in three different blends by means of model potential molecular dynamics (MPMD). The potential of such methods is largely unexplored and the dependence of miscibility on fullerene concentration or on the blend density is typically not taken into account in literature. Indeed, as polymer cells are processed from solution, typically by spin coating, fast drying of the blend layer occurs and generates nanoscale morphology in non-equilibrium conditions. Investigating equilibrium and also out-of-equilibrium conditions by varying the blend density in MPMD calculations may lead to better understanding of the formation processes of ternary blends.

In this work we determine the miscibility of PTB7, PTB7-th and Si-PCPDTBT with the fullerene-derivative $PC_{71}BM$, by calculating the mixing free energy as a function of the relative polymer:fullerene concentration and blend density. By calculating the variation in the free energy upon mixing each of the three polymers with the fullerene, we provide evidence that for high fullerene concentrations ($>$50%) and for dense blends PTB7 and PTB7-th are more miscible with fullerenes with respect to Si-PCPDTBT. This result suggests that when small amounts of the sensitizer are added to binary PTB7 (or PTB7-th) : $PC_{71}BM$ blends, it is unlikely that it will be located between the donor and the acceptor or within the fullerene phase, giving rise to a favorable BHJ architecture that can explain the improved FF experimentally measured. In addition, we show that these results depend on the blend density, and in particular that in case of low density blends the miscibility order can be altered. Since different densities are expected depending on the processing conditions, also different morphologies can be obtained.

2. Results and discussion

We calculate the free energy change $\Delta G_m/V_m$ upon mixing the polymers with the fullerene acceptor. The latter is defined as the free energy difference, per unit volume, between a blend and its separate components. It is a key thermodynamic parameter to measure the stability of mixtures and it is lower for more stable blends.

The free energy change is the sum of two contributions: the change in the enthalpy of mixing $\Delta H_m/V_m$, which is a measure of the energy change, and the change in configurational entropy $\Delta S_m/V_m$ times the temperature T:

$$\Delta G_m/V_m = \Delta H_m/V_m - T\Delta S_m/V_m \tag{1}$$

The change in configurational entropy is a known function of the concentration, and it can be calculated according to the Flory-Huggins theory[40, 41]. This is the appropriate theoretical framework to study the miscibility of macromolecules such as polymers, and it has been successfully applied to investigate the solubility of conjugated polymers for photovoltaics[42, 43].

The formula for the entropy change is:

$$\Delta S_m/V_m = -\frac{k_B}{V_0}\cdot\left[\phi_F\cdot\ln(\phi_F)+\frac{\phi_P}{r}\cdot\ln(\phi_P)\right] \tag{2}$$

where V_0 is a reference volume (we can choose it equal to the fullerene volume[14], i.e. 1.07 nm^3), ϕ_P and ϕ_F are the volume fractions of the polymer and the fullerene in the mix, and r is the volume of a polymer chain with respect to V_0. A typical value for the polymers used in these blends is $r \sim 100$[14], for which the value of $T\Delta S_m/V_m$ at room temperature is smaller than 1.5 MPa. As it will be shown below, this value is small with respect to the enthalpic contribution $\Delta H_m/V_m$ that dominates the miscibility at all concentrations. For completeness, the calculated $-T\Delta S_m/V_m$ and $\Delta G_m/V_m$ are reported in Supporting Information.

The enthalpic contribution can be calculated as

$$\frac{\Delta H_m}{V_m} = \mathrm{CED}_m - \phi_P(\mathrm{CED})_P - \phi_F(\mathrm{CED})_F \tag{3}$$

where V_m is the volume of the mix, and CED_m, CED_P and CED_F are the cohesive energy densities of the blend, pure polymer and pure fullerene phases, respectively. CED_P and CED_F are independent on ϕ and are calculated once for the pure polymer and fullerene phases by MPMD by building the crystalline bulks and calculating the corresponding cohesive energies per unit volume at equilibrium[42]. The calculated CED of pure phases, i.e. fullerene, PTB7[14], PTB7-th and Si-PCPDTBT are reported in Table 1.

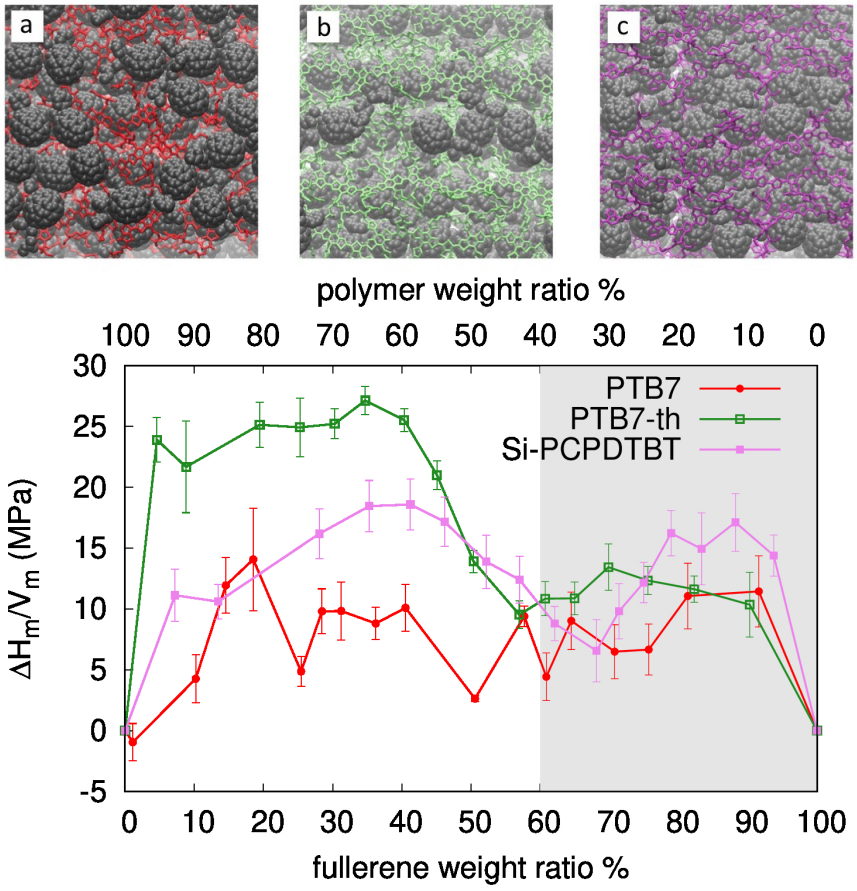

Figure 2: Top: 3D PTB7 (a), PTB7-th (b) and Si-PCPDTBT (c) :$PC_{71}BM$ blends used for the calculation of $\Delta H_m/V_m$. Bottom: $\Delta H_m/V_m$ calculated for different fullerene weight ratios. Error bars on each point are the standard deviation of the $\Delta H_m/V_m$ calculated on 10 systems with different starting configuration (see text). Grey shaded area corresponds to the polymer weight ratio used in Ref.26.

The values of $\Delta H_m/V_m$ are calculated at different relative concentration of fullerenes and are reported in Fig.2 (some data are taken from our previous work[14]). In order to calculate $\Delta H_m/V_m$, for each relative concentration, 10 starting configurations with different distribution of the fullerenes in the polymer matrix are considered, for a total of $\sim$500 structures, and annealed at room temperature and pressure for $\sim$20 ns. Each system contains $\sim 10^4$ atoms. From Fig. 2 we can observe that, excluding extreme values of concentration, the values of the enthalpy of mixing are always positive, meaning that the blends do not spontaneously form. Nevertheless, the local minima observed at specific concentrations (e.g. fullerene weight ratio of 50% for PTB7, 65% for PTB7-th and 68% for Si-PCPDTBT) allow to realize kinetically stable BHJs[14]. Mixing the fullerenes with PTB7 is more favorable (i.e. it has lower mixing enthalpy) than with Si-PCPDTBT at nearly all concentrations (red versus purple points in Fig. 2). The case of Si-PCPDTBT versus PTB7-th is less obvious since the corresponding $\Delta H_m/V_m$ curves intersect at several concentrations. However, we observe that for small amounts of sensitizer, i.e. fullerene weight ratio above 90%, corresponding to the experimental range of Ref.26, the value of $\Delta H_m/V_m$ is always quite high, i.e. the miscibility of Si-PCPDTBT with fullerenes is unfavoured with respect to the two other polymers. In the present work we do not simulate the whole ternary systems and the host-sensitizer interactions; nevertheless, the calculated lower miscibility of Si-PCPDTBT in fullerenes is already a robust indication that this polymer tends to stay separated from the fullerenes while PTB7 and PTB7th are energetically favored. Present results also show that increasing the sensitizer content is unfavorable for the desired morphology (see e.g. the low values of $\Delta H_m/V_m$ obtained for lower fullerene weight ratio around 70-65%, i.e. 30-35% Si-PCPDTBT weight ratio), as already pointed out in experiments.

In order to explain the dependence of $\Delta H_m/V_m$ on fullerene weight ratio (x) we consider a simple model based on the matching between the average fullerene-fullerene distance d and the polymer period L. The distance d depends on the fullerene weight ratio x and it can be obtained from the simulated systems as $d(x) = (V_m(x)/N(x))^{1/3}$ where $V_m(x)$ is the volume of the blend and $N(x)$ is the number of fullerenes. Assuming that that the miscibility is higher (i.e. $\Delta H_m/V_m$ is lower) when the fullerene spacing d matches the polymer periodicity L, i.e. d/L is an integer, we propose the following dependence on x

$$\frac{\Delta H_m(x)}{V_m(x)} \propto \left| \frac{d(x)}{L} - \left[\frac{d(x)}{L} \right] \right| \tag{4}$$

where $[\cdot]$ is the nearest integer function and $|\cdot|$ is the absolute value. This rough model (reported in Fig.3) is able to capture the main $\Delta H_m/V_m$ dependence on concentration, indicating the importance of matching the polymer periodicity to the fullerene-fullerene average distance. Beside this simple qualitative model based on donor-acceptor geometric commensurability, it is necessary to take into account specific physical factors such as blend density, polymer distortions, van der Waals and electrostatic interactions that contribute to the final miscibility of blends. This analysis is reported in Section 2.2.

2.1. Effect of non-equilibrium conditions

The results described in Fig. 2 are obtained in ideal conditions and at equilibrium density, but polymer blends are processed from solution using different solvents and deposition techniques. For example, spin coating leads to fast drying of the solvent during spinning[44] that forces the blend to adapt nanoscale morphologies under non-equilibrium conditions. The density of the blend is rapidly increased as the solvent evaporates and, at given density, the blend morphology starts to form. Another factor impacting the nanoscale morphology of the blend is the choice of the

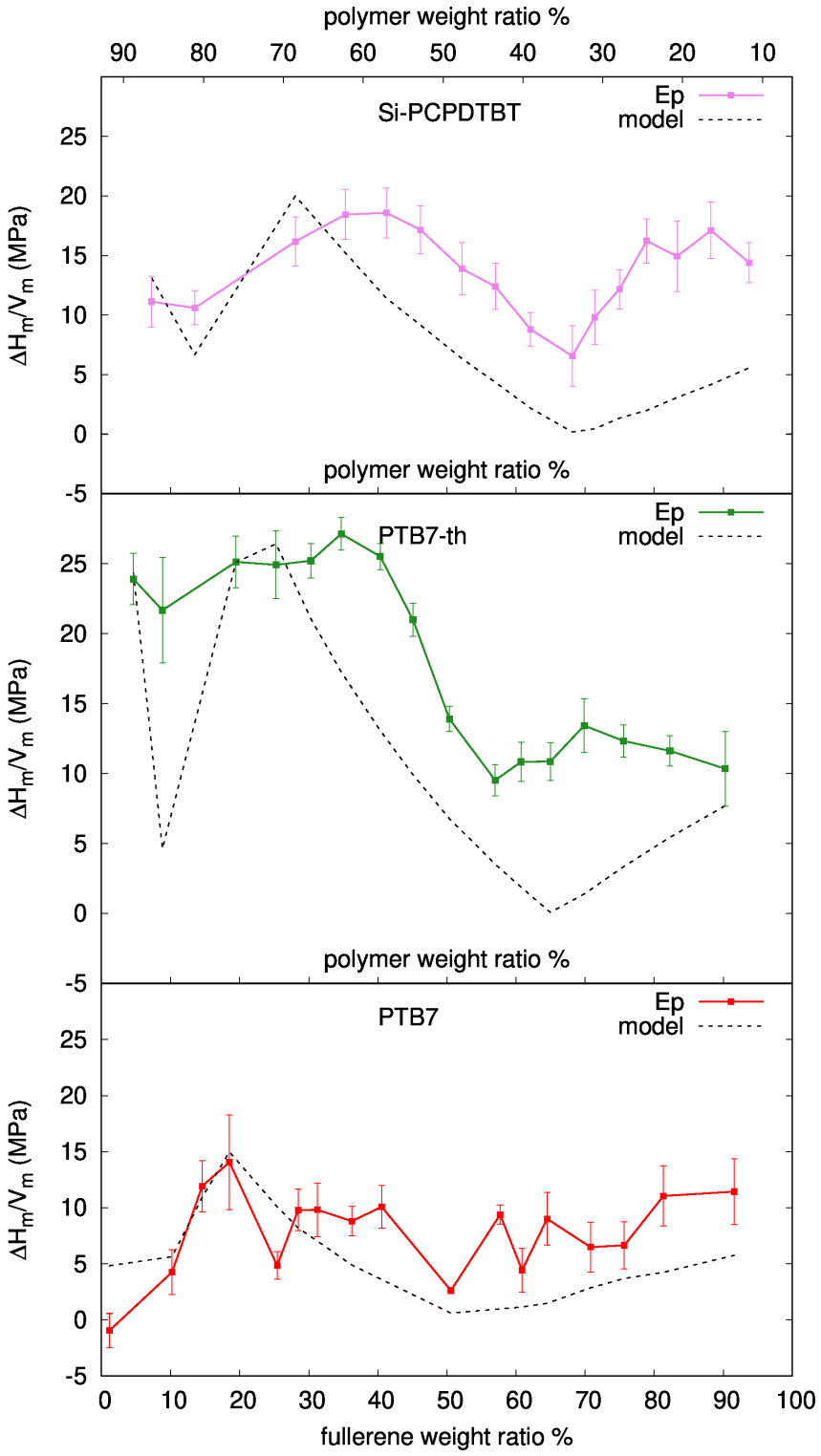

Figure 3: Enthalpy of mixing for the three polymers (solid lines) and mismatch model from Eq.4 (dashed lines). The values of L is used as an adjustable parameter and is chosen equal to 12.20 Å, 13.50 Å and 12.30 Å for Si-PCPDTBT, PTB7-th and PTB7, respectively, which compare well with the polymer periods in the perfect bulks. These are equal to 11.20 Å, 11.57 Å and 11.42 Å for Si-PCPDTBT, PTB7-th and PTB7, respectively.

solvent. For example, it has been shown that, depending on the chosen solvent, low-bandgap polymer P(NDI2OD-T2) can pre-aggregate in solution with important implications on semicrystalline morphology of the active layer of the devices[45, 46, 43]. In order to get more insight in the blend formation, we consider here the variation of blend density as a pre-state of blend formation under non-equilibrium conditions, which in turn may modify the enthalpy of mixing: less dense blends, for example, may allow the chains to relax in straighter configurations with lower strain energy. To investigate this effect, we have performed additional calculations on binary blends with fixed fullerene weight ratio (50%) and variable density ρ. The results are reported in Fig. 4 for $\sim 0.5\rho_0 < \rho < \rho_0$, where ρ_0 is the density of the blends of Fig. 2 (i.e. 1.30 g/cm^3 for PTB7:fullerene, 1.33 g/cm^3 for PTB7-th:fullerene and 1.19 g/cm^3 for Si-PCPDTBT:fullerene). At fixed polymer:fullerene weight ratio, the enthalpy of mixing depends on the density of the blend. The mixing enthalpy curve of Si-PCPDTBT:fullerene remains the highest at all densities; however it is worth noting that for less dense blends the PTB7th:fullerene mixing is favored with respect to PTB7:fullerene, .i.e. inverting their relative behavior with respect to the equilibrium density data of Fig. 2. This is an important result that shows the impact of density on the miscibility of the donor:acceptor pair and, in turn, on the final morphology of the blends obtained during non-equilibrium conditions occurring during layer processing. Of course, the calculations performed at variable density are not representative of all possible non-equilibrium conditions. On the other hand, simulating the complete synthesis process is out-of-reach for all-atom simulations. Nevertheless, our analysis at variable density gives useful indications at an affordable computational cost. To further understand the underlying mechanism governing the miscibility of the semiconductors, we discuss the free energy of mixing in more detail.

2.2. Microscopic analysis of the blends

In order to provide physical (i.e. microscopic) insight into the values of $\Delta H_m/V_m$ reported in Figs. 2 and 4, we have separated the different contributions of $\Delta H_m/V_m$ (also indicated as potential energy, E_p). In particular, we consider bonding (E_b), angular (E_a) and dihedral (E_d) contributions, that are two-, three- and four-body terms, respectively, describing the covalent chemical bonds among atoms of the molecules. The dihedral term E_d of a sequence of four-atoms can be explained as the energy cost associated to the displacement of the fourth atom out of the plane defined by the previous consecutive three atoms. We also separate the long-range dispersive van der Waals (E_v) and electrostatic (E_c) terms. The dihedral and van der Waals contributions are reported in Fig.5, while the remaining ones are reported in Fig. S1 of Supporting Information. The dispersive term is dominant for Si-PCPDTBT and PTB7, while the dihedral is dominant for PTB7-th. It is interesting that for PTB7-th the dispersive energy minima (at 25% and 65% fullerene weight ratio) correspond to dihedral energy maxima. This can attributed to the stiffness of the polymer; when PTB7-th and fullerenes are closely-packed the $\pi-\pi$ interactions are stronger (lowering dispersive energy) but the polymer chains undergo larger distortions (increasing the dihedral energy). This is confirmed also by the radial pair distribution functions g(r) (see Fig. S3 in SI) that indicates higher aggregation in PTB7-th.

Comparing PTB7-th and PTB7 we conclude that the presence of the thiophene unit enhances the $\pi-\pi$ polymer-fullerene interactions but increases the stiffness and energy cost of polymer torsions. This is consistent with the GAFF model[47] indicating larger forces for changing the angle between benzodithiophene and thiophene (involved in PTB7-th) than for that between benzodithiophene and ether group (involved in PTB7).

To further confirm the above results and better understand polymer-fullerene interactions at the

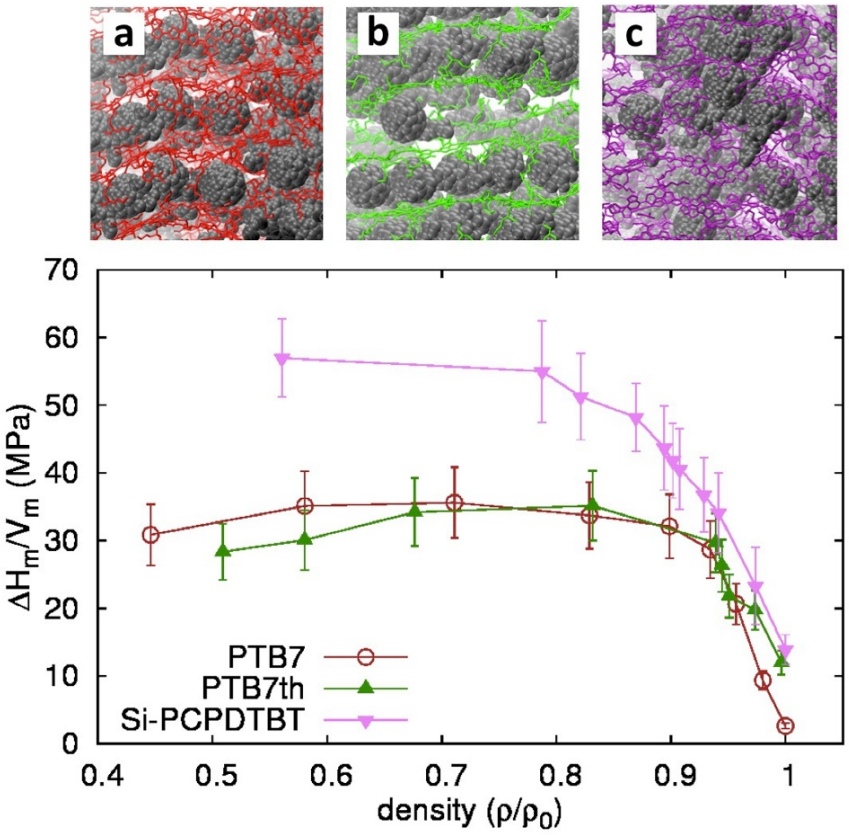

Figure 4: Top: examples of 3D PTB7 (a), PTB7-th (b) and Si-PCPDTBT (c) :$PC_{71}BM$ blends used for the calculation of $\Delta H_m/V_m$ at low density. Bottom: enthalpy of mixing at 1:1 polymer:fullerene concentration, calculated at different densities.

molecular level, we have simulated ideal polymer/fullerene systems with isolated polymer chains in order to (i) calculate the adhesion energy per fullerene unit and (ii) analyze the chain conformations close to the fullerenes. The model consists of an array of fullerenes in contact with two polymer chains. The simulation box contains four fullerenes and two monomers per chain (see Fig. S4 in SI). Since the polymeric systems have many configurations that are local minima for energy, we have relaxed (with a conjugated gradient minimization) a series of $\sim$100 configurations at varying initial relative position between the fullerenes and the polymer chain. The system with lowest configurational energy has thus been heated up to room temperature and simulated at ambient conditions for up to 50 nanoseconds. The adhesion energy is eventually calculated as the energy necessary to separate the polymers at infinite distance from the fullerenes. The results are reported in Table 1 and show that the highest adhesion to fullerenes is that of PTB7-th, followed by PTB7 and Si-PCPDTBT. As it can be seen from Fig. S4 (SI), these configurations correspond to a regular fullerene array, allowing the polymer chains to maximise interaction while keeping their backbones straight. When this condition is met, the cost of adhesion due to the polymer bending (dihedral contribution) is negligible, and adhesion of the more rigid PTB7-th is favoured.

By summarizing, we have found that the interaction of a single isolated polymer chain with fullerenes is maximum for PTB7-th due to strongest van der Waals forces compared to PTB7; on the contrary, for a dense 3D blend formed by assembling several polymer chains, PTB7 is favored and it is the most miscible to fullerenes. This trend further confirms the effect of the blend density described in Fig. 4, on the miscibility of PTB7 and PTB7-th with fullerene. At low density the

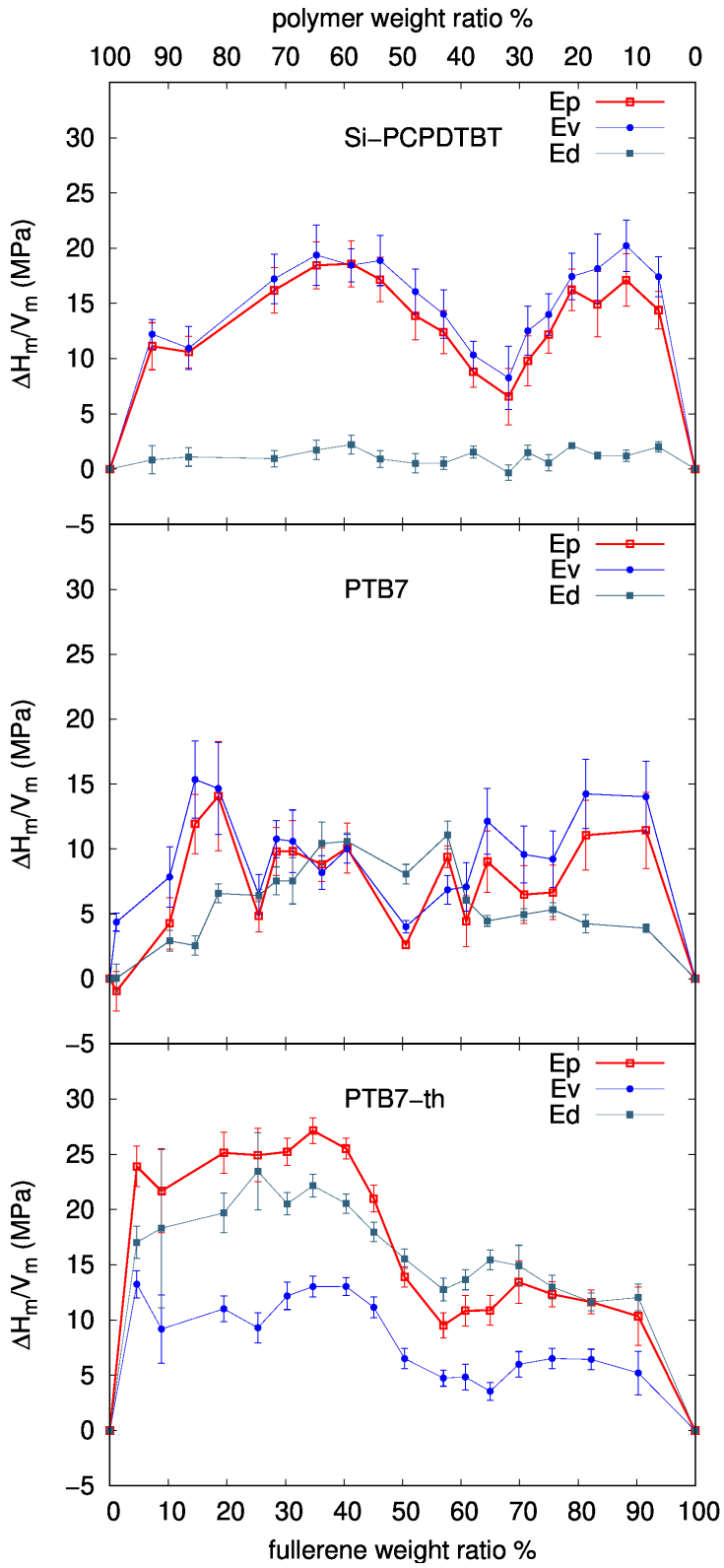

Figure 5: Dispersive van der Waals, E_v, and dihedral, E_d, contributions to mixing enthalpy $\Delta H_m/V_m = E_p$ for different fullerene weight ratios for PTB7-th:$PC_{71}BM$, PTB7:$PC_{71}BM$ and Si-PCPDTBT:$PC_{71}BM$ blends.

Table 1: Adhesion energy per fullerene unit between polymers and fullerenes (E_{adh}) and cohesive energy densities (CED) of polymers.

Polymer	E_{adh} (eV)	CED (MPa)
Si-PCPDTBT	-1.30	-244
PTB7	-1.93	-241
PTB7-th	-2.05	-255
$PC_{71}BM$	-	-391

PTB7-th chains are not sizably strained (bent) and the binding to fullerene is dominated by the large van der Waals interactions. As the density of the polymer/fullerene systems increases, the polymer chains are constrained by neighboring molecules (polymer chains and fullerenes) due to the cohesive forces in the blend. The energy cost of bending (dihedral term) increases rapidly for the more rigid PTB7-th so that the rather flexible PTB7 polymer is energetically favored and has better miscibility with fullerenes.

3. Conclusions

By using the Flory-Huggins theory, we have calculated through atomistic simulations the free energy of mixing of three polymer:fullerene blends as a function of their relative concentration and density. The chosen polymers are two hosts and one sensitizer used in highly efficient ternary organic solar cells. At experimental concentrations, the calculated free energy suggests that the sensitizer Si-PCPDTBT has the lowest miscibility to fullerenes and this is consistent with the sensitizer preferentially located far from the fullerenes. Since a hole transfer from the host to the sensitizer is expected, the predicted placement is able to deactivate hole traps and enhance the fill factor of the cell, as observed in experiments. The qualitative $\Delta H_m/V_m$ dependence on fullerene weight ratio is shown to be related to the matching between the average fullerene-fullerene distance and the polymer period. However, the detailed microscopic understanding of the miscibility requires to break down the enthalpy into different contributions. For PTB7-th blends we find a competition between the $\pi-\pi$ polymer-fullerene interaction and polymer torsional energy, which is not found in PTB7 and Si-PCPDTBT. Considering that the backbones of the polymers are very similar, we attribute these differences to the substitution of an oxygen atom in PTB7 with a thiophene unit in PTB7-th, which enhances the $\pi-\pi$ interactions but also promotes chain deformation. The investigation of blend density revealed that there are variations of the enthalpy of mixing as a function of the density, which indicates that different binary, but also ternary, blend morphology may generate depending on the deposition process, i.e. fast or slow layer drying, during which the blend will adapt non-equilibrium conditions. This results show that together with the polymer:fullerene weight ratio, the blend density can tune the relative ordering of the three moieties in the blends and, in turn, the morphology of the active layer.

4. Computational details

Model potential molecular dynamics simulations were performed by using the NAMD molecular simulations package (v. 2.9)[48]. The equations of motion of atoms were integrated by using the Velocity Verlet algorithm with a time step as small as 1 fs for constant volume and constant pressure (NVT/NPT ensemble) calculations. Multiple time stepping was used, with short-range

non bonded interactions calculated every two time steps and full electrostatics evaluated every 4 time steps. All the electrostatic contributions were computed by the Particle Mesh Ewald (PME) sum method, with PME grid spacing of 1 Å. Temperature was controlled by Langevin thermostat with damping coefficient. The host polymers and the fullerene were built with the code Avogadro (v. 1.0.3)[49] and described by the General Amber Force Field (GAFF)[47] successfully applied to study polymers and carbon allotropes, as well as their mix[50, 14]. For Si-PCPDTBT we have used the parameters from Guilbert et al.[51]. Atomic partial charges were calculated according to the standard AM1-BCC method[52]. Radial pair distribution functions were calculated with VMD package (v. 1.9)[53].

5. Acknowledgements

We acknowledge Italian MIUR for funding through project PON04a2 00490 M2M Netergit, PRACE for awarding access to Marconi KNL at CINECA, Italy, through projects DECONVOLVES (2018184466) and PROVING-IL (2019204911). CC acknowledges the CINECA award under the ISCRA initiative, for the availability of high performance computing resources and support (projects MITOMASC and UNWRAPIT). A.F. thanks "Progetti biennali d'Ateneo Finanziati dalla Fondazione di Sardegna 2017" (project n. F71I17000170002), and Project PRIN 2017 "TOPSPIN", funded by Italian Ministry of University and Research (MIUR). J.A. and C.V.A. acknowledge the French Research Agency for funding through the project NFA-15 (ANR-17-CE05-0020-01).

Notes and references

[1] R. G. Kepler, Charge carrier production and mobility in anthracene crystals, Phys. Rev. 119 (1960) 1226–1229. URL: https://link.aps.org/doi/10.1103/PhysRev.119.1226. doi:10.1103/PhysRev.119.1226.

[2] C. J. Brabec, N. S. Sariciftci, J. C. Hummelen, Plastic solar cells, Advanced functional materials 11 (2001) 15–26.

[3] S. Günes, H. Neugebauer, N. S. Sariciftci, Conjugated polymer-based organic solar cells, Chemical reviews 107 (2007) 1324–1338.

[4] O. Inganäs, Organic photovoltaics over three decades, Advanced Materials 30 (2018) 1800388.

[5] S. Chu, Y. Cui, N. Liu, The path towards sustainable energy, Nature materials 16 (2017) 16–22.

[6] R. Po, A. Bernardi, A. Calabrese, C. Carbonera, G. Corso, A. Pellegrino, From lab to fab: how must the polymer solar cell materials design change?–an industrial perspective, Energy & Environmental Science 7 (2014) 925–943.

[7] M. C. Scharber, On the efficiency limit of conjugated polymer:fullerene-based bulk heterojunction solar cells, Advanced Materials 28 (2016) 1994–2001. URL: https://onlinelibrary.wiley.com/doi/abs/10.1002/adma.201504914. doi:10.1002/adma.201504914. arXiv:https://onlinelibrary.wiley.com/doi/pdf/10.1002/adma.201504914.

[8] Y. Liu, J. Zhao, Z. Li, C. Mu, W. Ma, H. Hu, K. Jiang, H. Lin, H. Ade, H. Yan, Aggregation and morphology control enables multiple cases of high-efficiency polymer solar cells, Nature communications 5 (2014) 5293.

[9] K. Leo, Organic photovoltaics, Nat. Rev. Mater 1 (2016) 16056.

[10] M. Jorgensen, K. Norrman, S. A. Gevorgyan, T. Tromholt, B. Andreasen, F. C. Krebs, Stability of polymer solar cells, Advanced Materials 24 (2012) 580–612. URL: https://onlinelibrary.wiley.com/doi/abs/10.1002/adma.201104187. doi:10.1002/adma.201104187. arXiv:https://onlinelibrary.wiley.com/doi/pdf/10.1002/adma.201104187.

[11] N. Grossiord, J. M. Kroon, R. Andriessen, P. W. Blom, Degradation mechanisms in organic photovoltaic devices, Organic Electronics 13 (2012) 432 – 456. URL: http://www.sciencedirect.com/science/article/pii/S1566119911004046. doi:https://doi.org/10.1016/j.orgel.2011.11.027.

[12] P. Cheng, X. Zhan, Stability of organic solar cells: challenges and strategies, Chem. Soc. Rev. 45 (2016) 2544–2582. URL: http://dx.doi.org/10.1039/C5CS00593K. doi:10.1039/C5CS00593K.

[13] X. Yang, J. Loos, S. C. Veenstra, W. J. H. Verhees, M. M. Wienk, J. M. Kroon, M. A. J. Michels, R. A. J. Janssen, Nanoscale morphology of high-performance polymer solar cells, Nano Letters 5 (2005) 579–583. URL: https://doi.org/10.1021/nl048120i. doi:10.1021/nl048120i. arXiv:https://doi.org/10.1021/nl048120i, pMID: 15826090.

[14] S. B. Dkhil, M. Pfannmöller, M. I. Saba, M. Gaceur, H. Heidari, C. Videlot-Ackermann, O. Margeat, A. Guerrero, J. Bisquert, G. Garcia-Belmonte, A. Mattoni, S. Bals, J. Ackermann, Toward high-temperature stability of ptb7-based bulk heterojunction solar cells: Impact of fullerene size and solvent additive, Advanced Energy Materials 7 (2017) 1601486. URL: https://onlinelibrary.wiley.com/doi/abs/10.1002/aenm.201601486. doi:10.1002/aenm.201601486. arXiv:https://onlinelibrary.wiley.com/doi/pdf/10.1002/aenm.201601486.

[15] R. Cardia, G. Malloci, A. Mattoni, G. Cappellini, Effects of tips-functionalization and perhalogenation on the electronic, optical, and transport properties of angular and compact dibenzochrysene, Journal of Physical Chemistry A 118 (2014) 5170–5177. URL: https://www.scopus.com/inward/record.uri?eid=2-s2.0-84904561190&doi=10.1021%2fjp502022t&partnerID=40&md5=7e597df22f32a930690b80759c08b4f8. doi:10.1021/jp502022t.

[16] H. Wang, J. Huang, S. Xing, J. Yu, Improved mobility and lifetime of carrier for highly efficient ternary polymer solar cells based on tips-pentacene in ptb7: Pc71bm, Organic Electronics 28 (2016) 11 – 19. URL: http://www.sciencedirect.com/science/article/pii/S1566119915301518. doi:https://doi.org/10.1016/j.orgel.2015.10.009.

[17] T. Kumari, S. M. Lee, S.-H. Kang, S. Chen, C. Yang, Ternary solar cells with a mixed face-on and edge-on orientation enable an unprecedented efficiency of 12.1%, Energy & Environmental Science 10 (2017) 258–265.

[18] N. Gasparini, A. Salleo, I. McCulloch, D. Baran, The role of the third component in ternary organic solar cells, Nat Rev Mater 4 (2019) 229–242. doi:10.1038/s41578-019-0093-4.

[19] P. P. Khlyabich, B. Burkhart, B. C. Thompson, Compositional dependence of the open-circuit voltage in ternary blend bulk heterojunction solar cells based on two donor polymers, Journal of the American Chemical Society 134 (2012) 9074–9077.

[20] C. Wang, X. Xu, W. Zhang, S. B. Dkhil, X. Meng, X. Liu, O. Margeat, A. Yartsev, W. Ma, J. Ackermann, E. Wang, M. Fahlman, Ternary organic solar cells with enhanced open circuit voltage, Nano Energy 37 (2017) 24–31. URL: https://linkinghub.elsevier.com/retrieve/pii/S2211285517302719. doi:10.1016/j.nanoen.2017.04.060.

[21] Q. An, X. Ma, J. Gao, F. Zhang, Solvent additive-free ternary polymer solar cells with 16.27% efficiency, Science Bulletin 64 (2019) 504 – 506. URL: http://www.sciencedirect.com/science/article/pii/S2095927319301768. doi:https://doi.org/10.1016/j.scib.2019.03.024.

[22] T. Ameri, P. Khoram, T. Heumller, D. Baran, F. Machui, A. Troeger, V. Sgobba, D. M. Guldi, M. Halik, S. Rathgeber, U. Scherf, C. J. Brabec, Morphology analysis of near ir sensitized polymer/fullerene organic solar cells by implementing low bandgap heteroanalogue c-/si-pcpdtbt, J. Mater. Chem. A 2 (2014) 19461–19472. URL: http://dx.doi.org/10.1039/C4TA04070H. doi:10.1039/C4TA04070H.

[23] Y. M. Yang, W. Chen, L. Dou, W.-H. Chang, H.-S. Duan, B. Bob, G. Li, Y. Yang, High-performance multiple-donor bulk heterojunction solar cells, Nature photonics 9 (2015) 190.

[24] L. Yang, H. Zhou, S. C. Price, W. You, Parallel-like bulk heterojunction polymer solar cells, Journal of the American Chemical Society 134 (2012) 5432–5435.

[25] G. Mattioli, S. B. Dkhil, M. I. Saba, G. Malloci, C. Melis, P. Alippi, F. Filippone, P. Giannozzi, A. K. Thakur, M. Gaceur, O. Margeat, K. A. Diallo, A. Karim, C. VidelotAckermann, J. Ackermann, A. Amore Bonapasta, A. Mattoni, Interfacial engineering of p3ht/zno hybrid solar cells using phthalocyanines: a joint theoretical and experimental investigation, Advanced Energy Materials 4 (2014) 1301694.

[26] N. Gasparini, X. Jiao, T. Heumueller, D. Baran, G. Matt, S. Fladischer, E. Spiecker, H. Ade, C. Brabec, T. Ameri, Designing ternary blend bulk heterojunction solar cells with reduced carrier recombination and a fill factor of 77%, Nature Energy 1 (2016) 16118 EP –. URL: https://doi.org/10.1038/nenergy.2016.118. doi:Article.

[27] Y. Tang, H. Sun, Z. Wu, Y. Zhang, G. Zhang, M. Su, X. Zhou, X. Wu, W. Sun, X. Zhang, B. Liu, W. Chen, Q. Liao, H. Y. Woo, X. Guo, A new wide bandgap donor polymer for efficient nonfullerene organic solar cells with a large open-circuit voltage, Advanced Science 6 (2019) 1901773. URL: https://onlinelibrary.wiley.com/doi/abs/10.1002/advs.201901773. doi:10.1002/advs.201901773. arXiv:https://onlinelibrary.wiley.com/doi/pdf/10.1002/advs.201901773.

[28] M. Morana, H. Azimi, G. Dennler, H.-J. Egelhaaf, M. Scharber, K. Forberich, J. Hauch, R. Gaudiana, D. Waller, Z. Zhu, K. Hingerl, S. S. van Bavel, J. Loos, C. J. Brabec, Nanomorphology and charge generation in bulk heterojunctions based on low-bandgap dithiophene polymers with different bridging atoms, Advanced Functional Materials 20 (2010) 1180–1188. URL: https://onlinelibrary.wiley.com/doi/abs/10.1002/adfm.200900931. doi:10.1002/adfm.200900931. arXiv:https://onlinelibrary.wiley.com/doi/pdf/10.1002/adfm.200900931.

[29] Y. Liang, D. Feng, Y. Wu, S.-T. Tsai, G. Li, C. Ray, L. Yu, Highly efficient solar cell polymers developed via fine-tuning of structural and electronic properties, Journal of the American Chemical Society 131 (2009) 7792–7799. URL: https://doi.org/10.1021/ja901545q. doi:10.1021/ja901545q. arXiv:https://doi.org/10.1021/ja901545q, pMID: 19453105.

[30] S. C. Price, A. C. Stuart, L. Yang, H. Zhou, W. You, Fluorine substituted conjugated polymer of medium band gap yields 7% efficiency in polymer-fullerene solar cells, Journal of the American Chemical Society 133 (2011) 4625–4631. URL: https://doi.org/10.1021/ja1112595. doi:10.1021/ja1112595. arXiv:https://doi.org/10.1021/ja1112595, pMID: 21375339.

[31] H. J. Son, W. Wang, T. Xu, Y. Liang, Y. Wu, G. Li, L. Yu, Synthesis of fluorinated polythienothiophene-co-benzodithiophenes and effect of fluorination on the photovoltaic properties, Journal of the American Chemical Society 133 (2011) 1885–1894. URL: https://doi.org/10.1021/ja108601g. doi:10.1021/ja108601g. arXiv:https://doi.org/10.1021/ja108601g, pMID: 21265569.

[32] J. W. Jo, J. W. Jung, E. H. Jung, H. Ahn, T. J. Shin, W. H. Jo, Fluorination on both d and a units in d–a type conjugated copolymers based on difluorobithiophene and benzothiadiazole for highly efficient polymer solar cells, Energy & Environmental Science 8 (2015) 2427–2434.

[33] T. Wang, X.-K. Chen, A. Ashokan, Z. Zheng, M. K. Ravva, J.-L. Brédas, Bulk heterojunction solar cells: Impact of minor structural modifications to the polymer backbone on the polymer–fullerene mixing and packing and on the fullerene–fullerene connecting network, Advanced Functional Materials 28 (2018) 1705868.

[34] S. Bellani, M. Porro, C. Caddeo, M. I. Saba, P. B. Miranda, A. Mattoni, G. Lanzani, M. R. Antognazza, The study of polythiophene/water interfaces by sum-frequency generation spectroscopy and molecular dynamics simulations, J. Mater. Chem. B 3 (2015) 6429–6438. URL: http://dx.doi.org/10.1039/C5TB00388A. doi:10.1039/C5TB00388A.

[35] A. Sharma, L. Liu, S. Parameswaran, S. M. Grayson, H. S. Ashbaugh, S. W. Rick, Design of amphiphilic polymers via molecular dynamics simulations, The Journal of Physical Chemistry B 120 (2016) 10603–10610.

[36] I. V. Volgin, S. V. Larin, E. Abad, S. V. Lyulin, Molecular dynamics simulations of fullerene diffusion in polymer melts, Macromolecules 50 (2017) 2207–2218.

[37] D. J. Beltran-Villegas, A. Jayaraman, Assembly of amphiphilic block copolymers and nanoparticles in solution: coarse-grained molecular simulation study, Journal of Chemical & Engineering Data 63 (2018) 2351–2367.

[38] T. E. Gartner III, A. Jayaraman, Modeling and simulations of polymers: A roadmap, Macromolecules 52 (2019) 755–786.

[39] S. Ben Dkhil, P. Perkhun, C. Luo, D. Müller, R. Alkarsifi, E. Barulina, Y. A. Avalos-Quiroz, O. Margeat, S. T. Dubas, T. Koganezawa, et al., Direct correlation of nanoscale morphology and device performance to study photocurrent generation in donor enriched phases of polymer solar cells, ACS Applied Materials & Interfaces 12 (2020) 28404–28415. doi:10.1021/acsami.0c05884.

[40] M. L. Huggins, Solutions of long chain compounds, J. Chem. Phys. 9 (1941) 440–440. URL: http://link.aip.org/link/?JCP/9/440/1. doi:10.1063/1.1750930.

[41] P. J. Flory, Thermodynamics of high polymer solutions, J. Chem. Phys. 10 (1942) 51.

[42] C. Caddeo, A. Mattoni, Atomistic investigation of the solubility of 3-alkylthiophene polymers in tetrahydrofuran solvent, Macromolecules 46 (2013) 8003–8008. URL: https://doi.org/10.1021/ma401345n. doi:10.1021/ma401345n.

[43] C. Caddeo, D. Fazzi, M. Caironi, A. Mattoni, Atomistic simulations of p(ndi2od-t2) morphologies: From single chain to condensed phases, J. Phys. Chem. B 118 (2014) 12556–12565. URL: http://dx.doi.org/10.1021/jp5085789. doi:10.1021/jp5085789, pMID: 25264852.

[44] J. J. van Franeker, M. Turbiez, W. Li, M. M. Wienk, R. A. Janssen, A real-time study of the benefits of co-solvents in polymer solar cell processing, Nat. Commun. 6 (2015) 6229. URL: http://www.nature.com/articles/ncomms7229. doi:10.1038/ncomms7229.

[45] M. Schubert, D. Dolfen, J. Frisch, S. Roland, R. Steyrleuthner, B. Stiller, Z. Chen, U. Scherf, N. Koch, A. Facchetti, D. Neher, Influence of aggregation on the performance of all-polymer solar cells containing low-bandgap naphthalenediimide copolymers, Advanced Energy Materials 2 (2012) 369–380. URL: https://onlinelibrary.wiley.com/doi/abs/10.1002/aenm.201100601. doi:10.1002/aenm.201100601. arXiv:https://onlinelibrary.wiley.com/doi/pdf/10.1002/aenm.201100601.

[46] R. Steyrleuthner, M. Schubert, I. Howard, B. Klaumünzer, K. Schilling, Z. Chen, P. Saalfrank, F. Laquai, A. Facchetti, D. Neher, Aggregation in a high-mobility n-type low-bandgap copolymer with implications on semicrystalline morphology, Journal of the American Chemical Society 134 (2012) 18303–18317.

[47] J. Wang, R. M. Wolf, J. W. Caldwell, P. A. Kollman, D. A. Case, Development and testing of a general amber force field, J. Comput. Chem. 25 (2004) 1157–1174. URL: http://dx.doi.org/10.1002/jcc.20035. doi:10.1002/jcc.20035.

[48] J. C. Phillips, R. Braun, W. Wang, J. Gumbart, E. Tajkhorshid, E. Villa, C. Chipot, R. D. Skeel, L. Kalé, K. Schulten, Scalable molecular dynamics with namd, J. Comput. Chem. 26 (2005) 1781–1802. URL: http://dx.doi.org/10.1002/jcc.20289. doi:10.1002/jcc.20289.

[49] M. D. Hanwell, D. E. Curtis, D. C. Lonie, T. Vandermeersch, E. Zurek, G. R. Hutchison, Avogadro: An advanced semantic chemical editor, visualization, and analysis platform, Journal of Cheminformatics 4 (2012) 17.

[50] C. Caddeo, C. Melis, L. Colombo, A. Mattoni, Understanding the helical wrapping of p3ht on carbon nanotubes, J. Phys. Chem. C 114 (2010) 21109–21113.

[51] A. A. Guilbert, J. M. Frost, T. Agostinelli, E. Pires, S. Lilliu, J. E. Macdonald, J. Nelson, Influence of bridging atom and side chains on the structure and crystallinity of cyclopentadithiophene–benzothiadiazole polymers, Chemistry of Materials 26 (2014) 1226–1233.

[52] A. Jakalian, B. L. Bush, D. B. Jack, C. I. Bayly, Fast, efficient generation of high-quality atomic charges. am1-bcc model: I. method, J. Comput. Chem. 21 (2000) 132–146. URL: http://dx.doi.org/10.1002/(SICI)1096-987X(20000130)21:2<132::AID-JCC5>3.0.CO;2-P. doi:10.1002/(SICI)1096-987X(20000130)21:2<132::AID-JCC5>3.0.CO;2-P.

[53] W. Humphrey, A. Dalke, K. Schulten, Vmd: Visual molecular dynamics, J. Mol. Graphics 14 (1996) 33 – 38. doi:http://dx.doi.org/10.1016/0263-7855(96)00018-5.